Super-resolution upconversion microscopy of praseodymium-doped yttrium aluminum garnet nanoparticles

Roman Kolesov, Rolf Reuter, Kangwei Xia, Rainer Stöhr, Andrea Zappe, and Jörg Wrachtrup

3. Physikalisches Institut and Stuttgart Research Center of Photonic Engineering (SCoPE), Universität Stuttgart, Pfaffenwaldring 57, Stuttgart, D-70569, Germany

(Received 20 September 2011; published 31 October 2011)

We demonstrate background-free subdiffraction optical microscopy with upconverting YAG nanoparticles doped with trivalent praseodymium ions (Pr : YAG). The presented microscopy with Pr : YAG nanoparticles takes advantage of three facts. First, while excited with visible laser light, Pr : YAG nanoparticles can emit upconverted ultraviolet (UV) radiation, thus allowing for background-free microscopy. Second, the technique based on exploiting donut-shaped laser beam was introduced to obtain subdiffraction-limited optical resolution. All optical resolution of 50 nm limited by the size of the particles was achieved. Third, Pr : YAG nanoparticles are absolutely photostable. This technique resembles stimulated emission depletion microscopy (STED) though it is significantly different from STED since it involves stimulated absorption rather than stimulated emission.

DOI: 10.1103/PhysRevB.84.153413 PACS number(s): 78.67.Bf, 78.55.Qr, 87.64.kv

The resolution of conventional optical microscopy is limited by the wavelength of light being used. Abbe's limit sets the ultimate optical resolution to be $\lambda/2$ with λ being the wavelength of optical radiation used for imaging. However, many techniques recently introduced in fluorescent microscopy allow for breaking the diffraction limit. Those include stimulated emission depletion (STED)[1] and ground state depletion (GSD)[2] microscopies, stochastic image reconstruction based on photoswitchable fluorescers (STORM),[3] saturated structured illumination,[4] etc. The present work is concentrated around nonlinear laser microscopy techniques exploiting saturation of laser absorption or stimulated emission of fluorescent centers, primarily STED and GSD. Those were tested on a large number of fluorescent dye molecules and on photostable color centers in diamond.[5] The idea behind, for example, STED is to excite the fluorescent center with the laser of one color and try to immediately deplete the excited population by stimulating the center to emit with another laser having a donut-shaped beam profile with an intensity node. Under these circumstances, the center can fluoresce only if it is in the very node of the depleting donut-like beam. The reported all-optical resolution of STED lies in the range of 6–70 nm depending on the fluorescent species used.

On the other hand, upconversion emission of fluorescent centers is of high interest for microscopy because of the absence of a fluorescent background from the surrounding environment. Such techniques as coherent anti-Stokes Raman scattering (CARS)[6] and two-photon fluorescence excitation[7] are currently being used for microscopy. Recently, a new type of upconversion microscopy exploiting emission of rare-earth ions doped into crystalline nanoparticles has been introduced. It makes use of upconversion processes known in rare-earth doped laser materials for already a few decades. In particlular, nanoparticles of fluoride crystals co-doped with erbium and ytterbium[8,9] or with thulium and ytterbium[9,10] can emit green or blue light, respectively, under infrared excitation. On top of that, rare-earth ions are extremely photostable unlike dye molecules and, therefore, present robust fluorescent markers.

In our work, we combine the advantages of super-resolution optical microscopy techniques and the advantages of upconversion microscopy with rare-earth doped nanoparticles. Upconversion processes leading to UV fluorescence of trivalent praseodymium in yttrium aluminium garnet (YAG) are used for background-free optical imaging of Pr : YAG nanoparticles with the resolution ~50 nm, which is of the order of the size of the nanoparticles under study.

The structure of electronic levels of a Pr^{3+} ion in YAG is depicted in Fig. 1. The ground state of Pr^{3+} is the $^3H_4$ multiplet of the $4f^2$ electronic shell. Higher lying electronic states belonging to the same $4f^2$ shell give rise to parity-forbidden transitions from the ground state in absorption and to the ground state in emission. Those $4f^2 \leftrightarrow 4f^2$ optical transitions have low oscillator strengths ($\sim 10^{-7}$–10^{-5}), extremely weak coupling to phonons, and, therefore, long lifetimes ($\sim 10^{-5}$–10^{-3} s). However, higher lying states belonging to $4f5d$ shell give rise to parity allowed transitions to $4f^2$ states. The oscillator strengths of those transitions are much higher ($\sim 10^{-1}$–10^{-3}), and their coupling to phonons is much stronger. The latter results in wide absorption and fluorescence bands similar to the ones in organic dye molecules. The lowest $4f5d$ level is the only emitting state of Pr^{3+} because higher lying $4f5d$ levels rapidly decay into it nonradiatively. Its lifetime is reported to be ≈18 ns and its quantum efficiency is close to unity.[11] The emitted radiation covers the spectral range 300–450 nm.

There are at least two mechanisms of upconversion leading to UV emission under visible excitation. The first one studied in Ref. 12 relies on very efficient excitation of a Pr^{3+} ion into $^3P_0$ metastable state with a blue laser (the wavelengths can be 488 nm, 473 nm, 455 nm, etc.) followed by excitation into the second lowest $4f5d(2)$ level, subsequent nonradiative relaxation into the emitting $4f5d(1)$ state, and, finally, by emitting a UV photon.

The second way of upconversion reported in work[13] exploits excitation of a Pr^{3+} ion into its $^1D_2$ state by orange laser (≈609 nm) followed by the second excitation step directly into the emitting $4f5d(1)$ level by orange or green laser. The excited state absorption from the $^1D_2$ state is very inefficient at the wavelength of 609 nm since it terminates in the low energy tail of the $^1D_2 \rightarrow 4f5d(1)$ absorption band. Therefore,

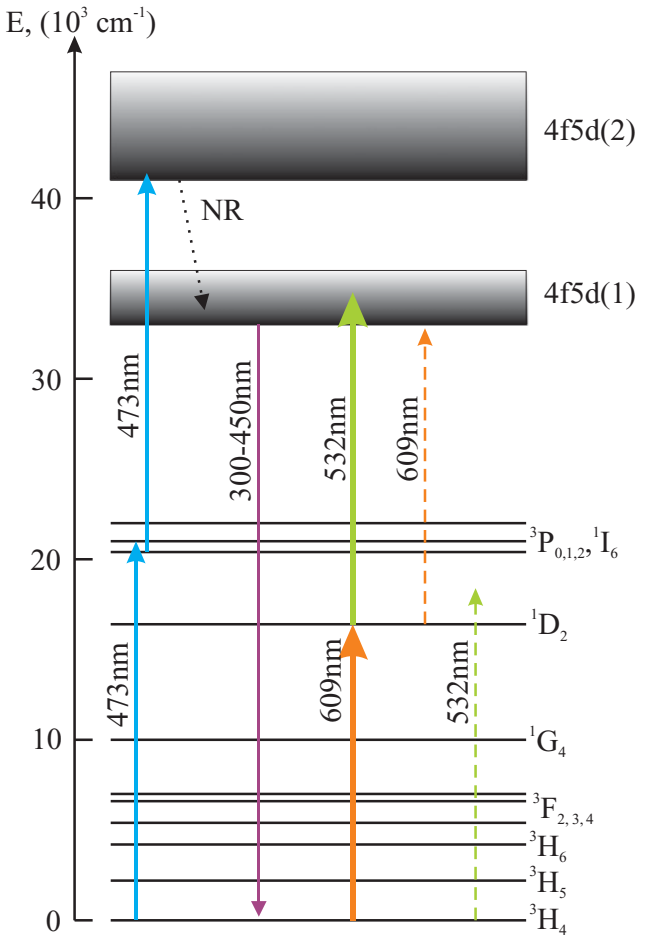

FIG. 1. (Color online) Energy level diagram of Pr^{3+} electronic states in YAG crystal. Two ways of stepwise excitation of upconverted UV fluorescence are shown. The excitation scheme used in the present work is indicated by bold arrows. It is also indicated that the second excitation step taken with a 609 nm laser hits the very edge of absorption into the $4f5d(1)$ state and that a 532 nm laser cannot serve as the first excitation step (indicated by dashed arrows).

the 609 nm laser primarily populates $^1D_2$ level rather than gives rise to efficient upconversion. However, the addition of 532 nm laser light increases the intensity of upconverted UV emission dramatically. The very same mechanism of two-step excitation was used in works[14] to demonstrate photon-gated photoconductivity at ambient conditions and holeburning in low-temperature Pr : YAG crystal. It will be used in the present work to demonstrate high-resolution microscopy of Pr : YAG nanoparticles.

Pr : YAG nanoparticles with a Pr doping concentration of 1% used in this study were synthesized by a sol-gel pyrolysis technique similar to a procedure reported for pure YAG.[15] The sample was characterized by x-ray diffraction (XRD) resulting in an average crystalline size of 32 nm. Confocal microscopy studies of Pr : YAG nanoparticles were performed in a home-built confocal microscope depicted in Fig. 2. A rhodamine 6G dye laser was used as an orange excitation source. The orange and green readout laser beams were passed through the same single-mode fiber to ensure their Gaussian beam profile and spatial overlap. Both beams

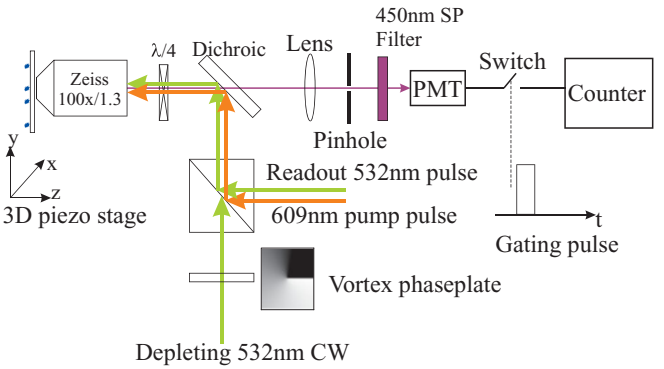

FIG. 2. (Color online) Confocal/super-resolution microscope used in the present study. The confocal studies of Pr : YAG nanoparticles were performed only with gaussian orange and green readout beams. Time-domain measurements were performed with all three beams being present, but with vortex plate taken out.

were sent onto the sample mounted on a three-dimensional nanopositioning piezo stage through a high numerical aperture oil immersion objective lens. The same objective lens was used to collect the emitted UV light which afterwards was filtered spatially with a pinhole and spectrally with a 450 nm shortpass filter and sent onto a UV-sensitive single-photon counting photomultiplier tube (PMT). A typical confocal scan of Pr : YAG nanoparticles spin-coated on a glass coverslip from an isopropanol suspension is shown in Figs. 3(a) and 3(c). The photon count rate of an emission from a single Pr : YAG particle was in the range of 100–200 counts/ms while the background was ~0.1 counts/ms. No change in the fluorescence intensity was observed after several hours of continuous illumination showing absolute photostability of Pr : YAG nanoparticles.

The confocal resolution in our case was ~400 nm (Gaussian full width). This value can be improved by at least an order of magnitude by taking advantage of the long lifetime of the intermediate $^1D_2$ state (≈150–200 μs[16]) and by exploiting a donut-shaped 532 nm beam as a second excitation step. In that situation, the population of $^1D_2$ level will be depleted by the donut green beam unless the particle is not in the very center of the donut. After that, the remaining population of $^1D_2$ state can be read out by a short 532 nm pulse. In the experiment, the orange excitation was chopped by an acousto-optic modulator while the depleting 532 nm beam was on all the time. After the orange excitation was switched off, the depleting beam was allowed to depopulate $^1D_2$ state for some time. Finally, a short readout Gaussian pulse of 532 nm wavelength was applied to the sample. The pulse sequence illuminating nanoparticles is indicated in Fig. 4 along with the fluorescence time traces corresponding to different powers of the Gaussian depleting beam. One can see that the intensity of upconversion induced by the readout pulse drops down dramatically as the power of the depleting beam is increased. The fluorescence decay after the readout pulse is shot is ≈20–22 ns, which is in good agreement with the known value of 18 ns. The exponential depletion rates after the orange laser is switched off depend linearly on the depleting laser intensity. This dependence allows us to predict the best achievable resolution once the depleting beam is donut-shaped in the following way. The

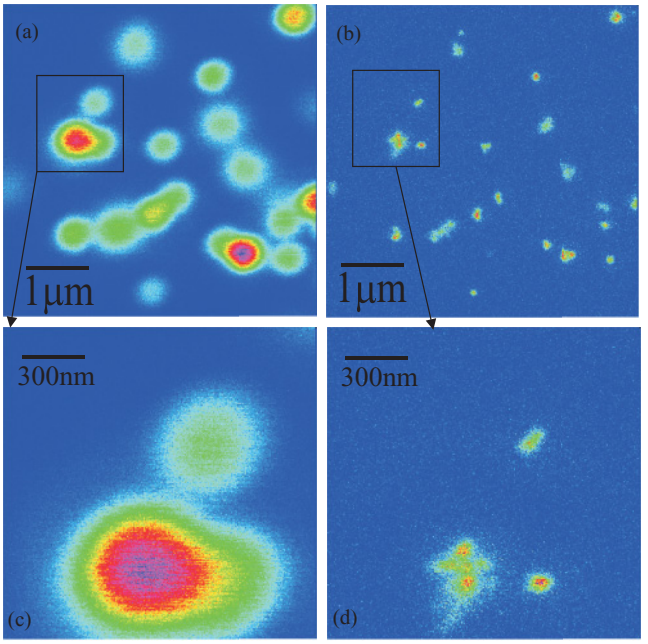

FIG. 3. (Color online) (a) Confocal image of Pr : YAG nanoparticles. (b) Super-resolution image of the same area. The parameters of the pulse sequence are as follows: 1) the total sequence duration was $\approx$6.8 μs corresponding to the repetition rate of 147 kHz, 2) the orange pulse duration was $\approx$1.3 μs with the unchopped orange power being $\approx$5 mW resulting in $\approx$1 mW of average orange pump power, 3) the delay between the green readout and the beginning of the consecutive orange pulse was $\approx$240 ns with the average readout power being 46 μW, 4) the power in the donut-shaped 532 nm depleting beam was $\approx$25 mW, 5) the readout gate was open for $\approx$80 ns starting $\approx$10 ns prior to the readout pulse arrival, and 6) dwell time per pixel was 3 ms. (c), (d) Confocal and super-resolution scans of a nanoparticle cluster. The shape of the nanoparticle aggregate can be retrieved. Images (a) and (c) were obtained under the same conditions as (b) and (d) only with the donut beam blocked.

radial intensity profiles of Gaussian and donut-like beams are given by the following expressions:

$$I_G = I_0 \exp\left(-\frac{r^2}{w^2}\right), \quad I_D = I_0 \frac{r^2}{w^2} \exp\left(-\frac{r^2}{w^2}\right). \qquad (1)$$

Here w is the Gaussian radius of the depleting green beam. The depletion rate as a function of radial distance is given by $\sigma I_{G,D}(r)$, where σ is the excited state absorption cross-section and depleting laser intensities are expressed in number of photons per unit time per unit area. After the period of time τ, the population remaining in $^1D_2$ state equals to $\rho_0 \exp(-\sigma I_{G,D}\tau)$, where ρ_0 is the population immediately after switching the orange laser off. Close to the node of the donut the remaining population will be

$$\rho \approx \exp(-\sigma I_0 \tau r^2/w^2). \qquad (2)$$

The value of $\sigma I_0 = \Gamma_0$ is exactly the depletion rate in the center of the Gaussian beam of the same power as the donut-like one. Thus, the best achievable resolution is given by

$$r_D = w/\sqrt{\sigma I_0 \tau} = w/\sqrt{\Gamma_0 \tau}. \qquad (3)$$

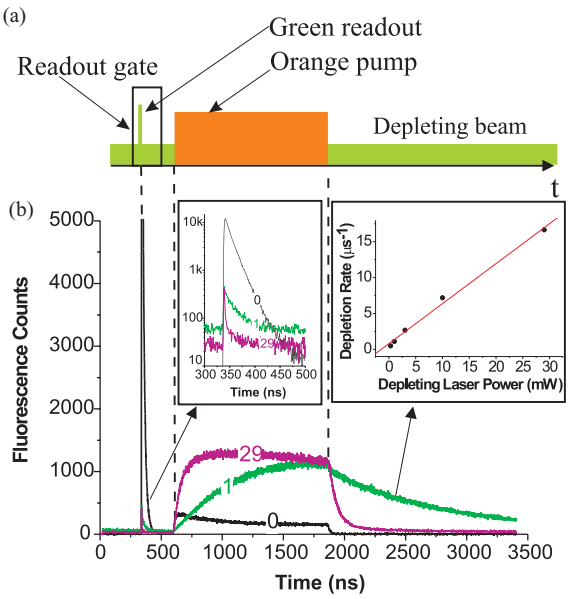

FIG. 4. (Color online) (a) Sequence of laser pulses used to evaluate the efficiency of intermediate state depletion by a 532 nm laser. (b) Time traces of fluorescence signals corresponding to the following powers of depleting beam: no depleting beam, 1 mW, and 29 mW at the input aperture of the objective lens. The right inset shows the depletion rate as a function of laser power while the left one demonstrates the decrease of signal produced by the readout pulse as the depleting beam becomes stronger.

As expected, the imaging resolution enhancement is proportional to the square root of depleting donut power and that of the dwell time τ between the end of the orange pulse and the green readout. For example, the 60 ns fluorescence decay time measured for $\approx$30 mW and $\tau = 5.3$ μs dwell time corresponding to the pulse sequence parameters being used would result in 9.4 times resolution enhancement and, correspondingly, in resolution of 42 nm (full Gaussian width).

To perform high-resolution imaging of Pr : YAG, the Gaussian orange pump and Gaussian green readout beams were combined with the donut-shaped depleting green beam on a beamsplitter and sent onto the sample containing Pr : YAG nanoparticles. At the same time, the PMT counts are gated so that the only photons contributing to the signal are the ones coming no longer than a few tens of nanoseconds after the readout pulse [see Fig. 4(a)].The high resolution scan of a 5×5 μm^2 area is shown in Fig. 3(b). In order to quantify the resolution improvement, images of a single Pr : YAG nanoparticle taken with different powers of the donut beam were analyzed (see Fig. 5). For low donut beam powers, the resolution follows the inverse square root dependence. However, it deviates from $1/\sqrt{P_{\text{donut}}}$ for high powers once the resolution reaches the nanoparticle size. The Gaussian full width of the super-resolution image was found to be 54 nm at 29 mW of the donut power. It was also noticed that increasing the power of the depleting donut beam as well as increasing waiting time between the orange pump and green readout pulses leads to a significant drop of the

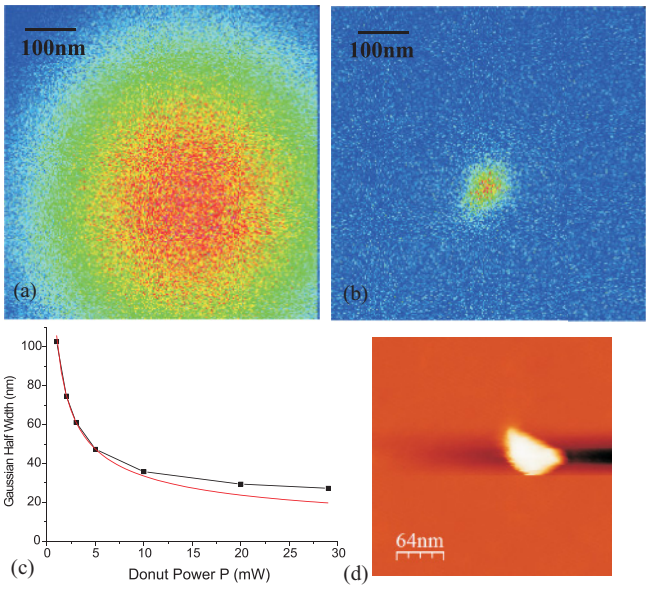

FIG. 5. (Color online) (a) Confocal image of a single nanoparticle. (b) High resolution image of the same nanoparticle. The power of the donut beam used was 29 mW. (c) The dependence of the Gaussian half width of high resolution fluorescent spot as a function of donut beam power. The lower curve represents $1/\sqrt{P}$ fit of the low donut power data points. The resolution dependence clearly deviates from $1/\sqrt{P}$ for high P. (d) AFM image of the same particle revealing its ≈33 nm height and 40–50 nm lateral size.

fluorescence signal. The most probable cause of both effects is that the donut beam is leaking inside the nanoparticle because of the refractive index mismatch between air and YAG ($n = 1.82$).

In order to demonstrate the resolving power of the discussed technique, a super-resolution scan of a cluster of nanoparticles has been taken. The confocal and super-resolution images are compared in Figs. 3(c) and 3(d). Sub-100 nm features of the cluster can be clearly resolved on Fig. 3(d) while the confocal image shows only a structureless bright spot.

In conclusion, we have demonstrated super-resolution background-free optical microscopy of upconverting Pr : YAG nanoparticles. The best resolution obtained so far was ∼50 nm and is limited by the nanoparticle size. YAG-based materials are known to be nontoxic for cells[17] and, therefore, Pr : YAG nanoparticles are very good candidates for nanoscale background-free intracellular imaging. The emitted UV radiation of Pr^{3+} ions is substantially red shifted with respect to the UV action spectrum for cell killing[18] and, therefore, in small doses can be considered harmless. The demonstrated method of nanoscale upconversion imaging exploiting depletion of an intermediate electronic state can be implemented with other prospective photostable rare-earth doped upconverting markers having emission wavelength in the visible range.

The work was financially supported by Volkswagenstiftung and Baden-Württemberg Stiftung.

[1] S. W. Hell and J. Wichmann, Opt. Lett. **19**, 780 (1994); S. W. Hell, Science **316**, 1153 (2007).
[2] E. Rittweger, D. Wildanger, and S. W. Hell, Europhys. Lett. **86**, 14001 (2009).
[3] M. J. Rust, M. Bates, and X. Zhuang, Nature Methods **3**, 793 (2006); B. Huang, W. Wang, M. Bates, and X. Zhuang, Science **319**, 810 (2008).
[4] M. G. L. Gustafsson, Proc. Natl. Acad. Sci. **102**, 13081 (2005).
[5] For the list of fluorescent dyes being used for STED and the corresponding references see webpage [http://www.mpibpc.mpg.de/groups/hell/STED_Dyes.html].
[6] C. L. Evans and X. S. Xie, Annu. Rev. Anal. Chem. **1**, 883 (2008).
[7] W. Denk, J. H. Strickler, and W. W. Webb, Science **248**, 73 (1990).
[8] S. Wu, G. Han, D. J. Milliron, S. Aloni, V. Altoe, D. V. Talapin, B. E. Cohen, and P. J. Schuck, Proc. Natl. Acad. Sci. **106**, 10917 (2009).
[9] J.-C. Boyer, L. A. Cuccia, and J. A. Capobianco, Nano Lett. **7**, 847 (2007).
[10] G. Chen, T. Y. Ohulchanskyy, R. Kumar, H. Agren, and P. N. Prasad, ACS Nano **4**, 3163 (2010).
[11] M. J. Weber, Solid State Commun. **12**, 741 (1973).
[12] J. Ganem, W. M. Dennis, and W. M. Yen, J. Lumin. **54**, 79 (1992).
[13] S. K. Gayen, B. Q. Xie, and Y. M. Cheung, Phys. Rev. B **45**, 20 (1992).
[14] R. M. Macfarlane and G. Wittmann, Opt. Lett. **21**, 1289 (1996); G. Wittmann and R. M. Macfarlane, *ibid.* **21**, 426 (1996).
[15] P. Vaqueiro and M. A. Lopez-Quintela, J. Mater. Chem. **8**, 161 (1998).
[16] G. Özen, O. Forte, and B. Di Bartolo, Opt. Mater. **27**, 1664 (2005).
[17] The nontoxic nature of Ce : YAG particles was mentioned in, for example, work by R. Asakura, T. Isobe, K. Kurokawa, H. Aizawa, and M. Ohkubo, Anal. Bioanal. Chem. **386**, 1641 (2006). Our own toxicity tests performed on HeLa cells showed no cell death caused by Pr : YAG nanoparticles upon incubating the cells in the buffer containing Pr : YAG solution for 24 hours.
[18] T. Okuno, Industrial Health **45**, 137 (2007).